

Dynamical Decoupling of Spin-Clusters using Solid State NMR

Abhishek Shukla and T. S. Mahesh*

NMR Research Center, Indian Institute of Science Education and Research (IISER), Pune 411008, India

(Dated: January 22, 2022)

In this work we experimentally study the efficiency of various dynamical decoupling sequences for suppressing decoherence of single as well as multiple quantum coherences on large spin-clusters. The system involves crystallites of a powdered sample containing a large number of molecular protons interacting via long-range dipole-dipole interaction. The multiple quantum coherences are prepared by progressively creating correlations in the spin lattice using standard pulse sequences implementing two-quantum average Hamiltonian. The spin system is then subjected to various dynamical decoupling sequences, followed by conversion into observable single quantum coherence by using time-reversal sequence. The experiments reveal superior performance of the recently introduced RUDD sequences in suppressing the decoherence.

PACS numbers: 03.67.Lx, 03.67.-a, 76.30.-v

Keywords: Quantum information, decoherence, dynamical decoupling, nuclear magnetic resonance, multiple quantum coherence

I. INTRODUCTION

The study of dynamics and control of quantum many body systems has renewed interest in the field of quantum information. While encoding information onto a quantum channel can potentially speed up certain computations and allow secure data transmission, the practical realization of these applications are hindered by the extreme sensitivity of the quantum channel to environmental noises. Systems based on nuclear spin-clusters is one among the various architectures being investigated to realize quantum channels. Several experimental demonstrations of quantum information processing (QIP) using solid-state nuclear magnetic resonance (SSNMR) have already been reported [1–5]. By sophisticated control of spin-dynamics it is in principle possible to achieve a larger number of quantum bits (qubits) using SSNMR, because of the availability of large spin-clusters coupled mutually through long-range dipole-dipole interactions. However in such a spin-cluster, fluctuating local fields at the site of each spin induced by its environment leads to the decoherence of the encoded quantum information.

Due to the availability of large spin-clusters it is possible to prepare coherences of large quantum numbers by a widening network of correlated spins evolving under two-quantum average Hamiltonian [6, 7]. These higher order coherences are not directly observable as macroscopic magnetizations, but can be converted into observable single quantum coherence (SQC) using a time-reversed two-quantum average Hamiltonian. This method, often known as a ‘spin-counting experiment’ has been used to study the evolution of coherences of large quantum numbers exceeding 4000 [8–10].

Under the standard Zeeman Hamiltonian any spin-coherence is a non-equilibrium state and decays via var-

ious relaxation processes, ultimately leading to the equilibrium longitudinal magnetization. It has long been discovered that the decay process of the spin coherence can be prolonged by applying a series of spin flips at regular intervals of time. This sequence known as ‘CPMG sequence’, not only refocuses the effect of spectrometer inhomogeneities, but also reverses the phase evolution of the coherences under the random fluctuations, provided the spin flips are applied sufficiently frequent [11, 12]. Such a dynamical method for the suppression of decoherence of a qubit due to its interaction with environment is often termed as ‘dynamical decoupling’ (DD) [13]. Recently Uhrig introduced a non-periodic spin-flip sequence which he proved theoretically to provide optimal decoupling performance for dephasing spin-bath interactions [14]. CPMG and other similar periodic spin-flip sequences suppress spin-environment interaction to n th order using up to $O(2^n)$ pulses, while Uhrig dynamical decoupling (UDD) suppresses the same using only n pulses. Filter function analysis of dynamical decoupling indicates that, in a high frequency dominated bath with a sharp cutoff, UDD works well provided the frequency of the spin-flips exceeds the cutoff frequency [15–17]. On the other hand when the spectral density of the bath has a soft cutoff (such as a broad Gaussian or Lorentzian), the CPMG sequence was found to outperform the UDD sequence [18–25]. Later on, UDD has been generalized to suppress simultaneously both transverse dephasing and longitudinal relaxation of a qubit [26]. Also, the original sequence for UDD is based the assumption of instantaneous spin-flips, which requires infinite bandwidth. More recently, Uhrig provided an improved sequence - ‘realistic UDD’ (RUDD) for practical implementations with finite bandwidth [27].

Most of the theory and experiments of DD sequences are for single spin systems. Du et al have studied DD of electron spin coherence in solids [18], while Suter and co-workers have reported systematic experimental comparisons of various DD schemes on an ensemble of single

*Electronic address: mahesh.ts@iiserpune.ac.in

spins in SSNMR [19, 25].

Later Agarwal has shown using theoretical and numerical calculations that even entangled states of two-qubit systems can be stored more efficiently using UDD [28]. Similar theoretical studies were also carried out by Mukhtar et. al. [29]. Experimentally, Wang et. al. have studied DD on electron-nuclear spin pairs in a solid-state system [30], and Soumya et. al. have studied the performance of UDD on a two-qubit liquid-state NMR system [31].

In this article, we report the experimental study of performance of various DD schemes on an extended network of spin-1/2 nuclei forming a large spin cluster. This article is organized as follows. Next section briefly describes the method of preparing and detecting multiple quantum coherences (MQC) in SSNMR, section III summarizes the construction of various DD sequences, and the experimental details are described in section IV. Finally we conclude in section V.

II. MULTIPLE QUANTUM SSNMR

The SSNMR Hamiltonian for a spin cluster with M spin-1/2 nuclei is

$$\mathcal{H}_{int} = \mathcal{H}_Z + \mathcal{H}_D, \quad (1)$$

where the Zeeman and the secular part of dipolar interaction are respectively,

$$\begin{aligned} \mathcal{H}_Z &= \sum_{i=1}^M \omega_i I_z^i, \\ \mathcal{H}_D &= \sum_{i < j} D_{ij} [3I_z^i I_z^j - \mathbf{I}^i \cdot \mathbf{I}^j] \end{aligned} \quad (2)$$

[32]. Here \mathbf{I}^i and I_z^i are spin angular momentum operator and its z-component corresponding to the i^{th} spin, and w_i and D_{ij} are the chemical shift and the dipolar coupling constants. The equilibrium density matrix for the above Hamiltonian corresponds to the longitudinal magnetization expressed as $\sum_i I_z^i$. The density matrices for the longitudinal spin order can be expressed using product of longitudinal spin operators, eg. $I_z^1 I_z^2 \dots$. The coherences are described by the product of transverse (or of transverse and longitudinal) spin operators, eg. $I_x^1 I_x^2 I_x^3 \dots$. The transverse spin operators can also be expressed in terms of raising and lowering operators: $I_x = (I_+ + I_-)/2$ and $I_y = -i(I_+ - I_-)/2$. The difference between the total number of raising and lowering operators gives the quantum number n of a particular coherence. For example, operators $I_+^j I_-^k$, I_+^j , and $I_+^j I_+^k$ describe zero, single, and two-quantum coherences respectively [33].

The pulse sequence for preparing and detecting MQC is shown in Fig. 1(a-b). The sequence in Fig. 1a involves preparation of MQC, application of DD schemes, free-evolution (t_1), converting MQC into longitudinal spin order (mixing), destroying the residual coherences by trans-

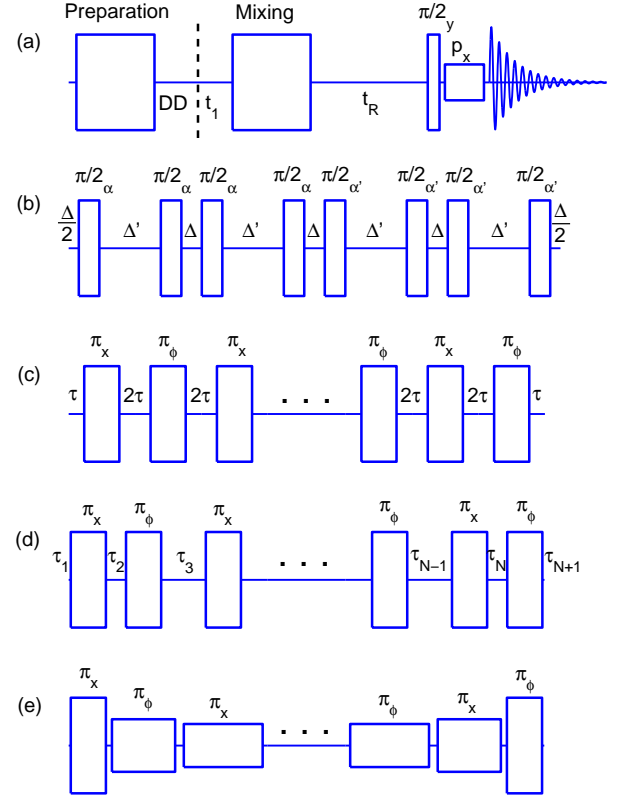


FIG. 1: The experimental scheme (a) for studying the performance of DD on large spin-clusters and the 8-pulse sequence (b) implementing $\mathcal{H}_1(\alpha)$. In (b), $\Delta' = 2\Delta + \tau_{\pi/2}$, where $\tau_{\pi/2}$ is the duration of each $\pi/2$ pulse. The DD schemes are described in (c-e). The phase ϕ is set to x for CPMG, UDD, and RUDD schemes, while it is alternated between x and $-x$ for CPMGp, UDDp, and RUDDp.

verse relaxation (t_R), followed by detection after converting the longitudinal spin order into SQC. The 8-pulse sequence in Fig. 1b corresponds to the two-quantum average Hamiltonian

$$\mathcal{H}_1 = \frac{D_{ij}}{2} (I_+^i I_+^j + I_-^i I_-^j), \quad (3)$$

for $\alpha = 0$. Preparation and mixing parts involve m -cycles of the 8-pulse sequence $\mathcal{H}_m(\alpha)$ and $\mathcal{H}_m(\pi/2)$ [7]. Under the preparation sequence, each uncorrelated spin gets correlated with its neighboring spins, creating two-quantum coherence. Each pair of correlated spins evolve under their neighbors, and this growing network of correlated spins in the form of higher order coherences leads to large correlated clusters. The possible quantum numbers and the corresponding cluster size increases with the number of cycles. Only even quantum coherences are prepared as shown in Fig. 2. However, MQCs themselves have no detectable macroscopic observables. MQCs can be converted back to longitudinal spin order by a time-reversal sequence $\mathcal{H}_m(\pi/2)$ (mixing), and subsequently be converted into detectable SQCs by a $\pi/2_y$ pulse. To

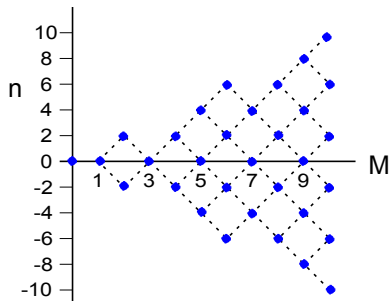


FIG. 2: Possible quantum numbers (n) for M -spin cluster after excitation with several cycles of 8-pulse sequence (Fig. 1b) implementing two-quantum average Hamiltonian (\mathcal{H}_m).

separate the MQCs, the relative phase α between the preparation and mixing is incremented in proportion to the evolution time t_1 (Fig. 1a). Spurious transverse coherences are suppressed by an extended delay t_R . A final purge pulse p_x is used to keep only the x -component.

III. DD SCHEMES

A. CPMG and CPMGp

CPMG and CPMGp schemes involve periodic spin flips as shown in Figure 1(c). The phase ϕ is set to x in CPMG, while it is alternated between x and $-x$ in CPMGp. CPMG and CPMGp have different performances depending on the initial states [19, 34, 35]. The total duration of the N -pulse CPMG is $T = N(2\tau + \tau_\pi)$, where 2τ is the delay between the π pulses and τ_π is the duration of each π pulse. The same parameters N and T are used to compare CPMG with the following schemes.

B. UDD and UDDp

The pulse distributions for UDD and UDDp schemes are shown in Fig. 1(d). Here the spin flips are symmetric but not periodic [14]. The j^{th} π pulse is applied at the time instant

$$t_j = T \sin^2 \left[\frac{\pi j}{2N + 2} \right], \quad (4)$$

where T is the total duration of the sequence and N is the total number of pulses. For a finite bandwidth case, with a π pulse of duration τ_π , the delays τ_j are given by $\tau_1 = \tau_{N+1} = t_1 - \tau_\pi/2$, $\tau_j = t_{j+1} - t_j - \tau_\pi$, for $2 \leq j \leq N$. Like in the previous scheme, UDD and UDDp are differed by the constant phase and the phase alternation in ϕ .

C. RUDD

In RUDD and RUDDp, in addition to the delays between the pulses, the pulse durations and amplitudes also vary, but the overall sequence remains symmetric [27]. The pulse durations are given by

$$\tau_\pi^j = T \left[\sin \left(\frac{\pi j}{N + 1} \right) \sin \theta_p \right], \quad (5)$$

where T is total duration of the sequence and N is the number of pulses. Here θ_p is a constant and can be determined by the allowed bandwidth. We choose $\tau_\pi^1 = \tau_\pi$, and calculated θ_p based on the minimum allowed pulse duration:

$$\sin \theta_p = \frac{\tau_\pi}{T \sin \left(\frac{\pi}{N+1} \right)}. \quad (6)$$

The amplitude a_j of j^{th} pulse is calibrated such that $2\pi a_j \tau_\pi^j = \pi$. Time instants of the center of each pulse is same as in equation (4). Using these time instants, the delays between the pulses can be calculated as $\tau_1 = \tau_{N+1} = t_1 - \tau_\pi/2$, and $\tau_j = t_j - t_{j-1} - \tau_\pi^j/2 - \tau_\pi^{j-1}/2$ for $2 \leq j \leq N$. Like in the previous schemes, RUDD and RUDDp are differed by the constant phase and the phase alternation in ϕ .

IV. EXPERIMENT

The sample consists of crystallites of powdered hexamethylbenzene. At room temperature the entire molecule undergoes six fold hopping about the C_6 axis of benzene ring [7]. Further the methyl group rapidly reorients about its C_3 axis. Due to these motions, the intramolecular dipolar interactions are averaged out. Intermolecular dipolar coupling is retained and each molecule acts as a point dipole [7]. Under free precession (no DD), this sample has a spin-spin relaxation constant of about 25 μs and a spin-lattice relaxation constant of 1.7s. All the experiments are carried out on a Bruker 500 MHz spectrometer at room temperature.

A. DD on SQC

First we describe the performance of various DD schemes on SQC. SQC was prepared by using an initial $(\pi/2)_y$ pulse on equilibrium longitudinal magnetization. As described in section and Fig. 1c, CPMG sequences were constructed by periodic distribution of π pulses in $\tau - \pi - \tau$ fashion. The minimum τ in our experiments was set to 2 μs owing to the duty cycle limit of the probe coil. Also duration of π pulse was found to be $\tau_\pi = 4.3 \mu\text{s}$ at maximum allowed amplitude. Under these experimental conditions, the allowed values of N for UDD and RUDD are 1 to 7. For $N \geq 8$, one obtains

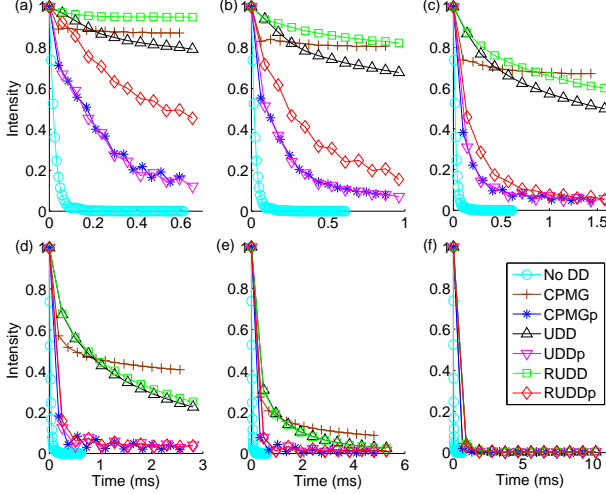


FIG. 3: Performance of 7-pulse DD cycles on SQC. The graphs correspond to $\tau = 2 \mu\text{s}$ (a), $\tau = 4 \mu\text{s}$ (b), $\tau = 8 \mu\text{s}$ (c), $\tau = 16 \mu\text{s}$ (d), $\tau = 32 \mu\text{s}$ (e), and $\tau = 64 \mu\text{s}$ (f).

negative delays between the pulses. Therefore to study DD schemes for longer durations, we cycled these 7-pulse DD sequences. The 7-pulse CPMG has a total cycle time of $T(\tau) = 7(2\tau + \tau_\pi)$. The results of these experiments are shown in Fig. 3. The graphs correspond to τ values ranging from $2 \mu\text{s}$ to $64 \mu\text{s}$. The corresponding $T(\tau)$ values are used to select the sampling points in no DD, as well as to construct other DD sequences. It is clear from these data that RUDD displays superior performance for shorter τ values, while CPMG shows better performance for longer τ values. We can also notice from these plots that the performance of RUDDp is better than CPMGp and UDDp which have almost same performance. UDD has better behavior than RUDDp, and for longer τ values UDD and RUDD have same behavior. However, these performances in general may also be dependent on initial states [19].

B. DD on MQC

As described in section II and Fig. 1(a-b), the scheme for studying DD on MQC involves preparation of MQC, evolution of MQC, followed by storing MQC onto longitudinal spin-orders. A delay $t_R = 5 \text{ ms}$ allows spurious coherences to decay. The longitudinal spin order is then converted into SQC using a $(\pi/2)_y$ pulse, followed by a purge pulse p_x of duration $50 \mu\text{s}$. A 180 degree phase alternation of the detection pulse, purge pulse, and the receiver is used to reduce artifacts arising from receiver ringing [7]. For efficient generation of MQC five cycles of 8-pulse sequence shown in Fig. 1b was used in preparation and mixing periods, and the parameter Δ was optimized to $2 \mu\text{s}$. In our experiments

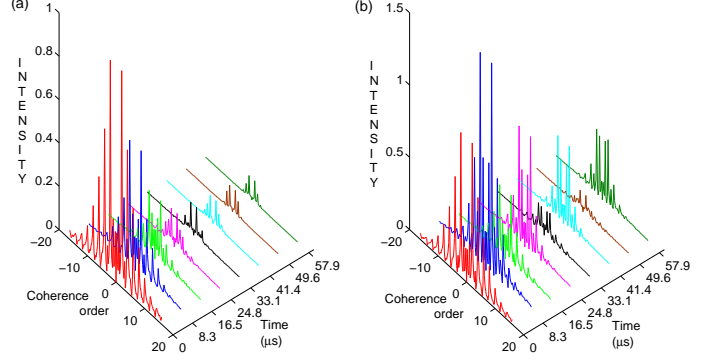


FIG. 4: Multiple quantum spectra showing different coherence orders detected after inserting different delays (a) and RUDD sequences of same durations (b).

the coherences of successive quantum numbers are separated by $\Delta\omega = 2\pi \times 200 \text{ kHz}$. In order to separate a maximum of n_{max} coherences, the relative phase α between the preparation and mixing is incremented by $\Delta\alpha = \pi/n_{\text{max}}$, where n_{max} was chosen to be 64. The corresponding increment in the evolution period is given by $\Delta t_1 = \Delta\alpha/\Delta\omega$. The signal intensities of the spectrum corresponding to these increments after cosine transform display strong peaks at even multiples of $\Delta\omega$. Mean value of the signal intensities is made to zero to suppress strong zero-quantum peak. Fig. 4a displays these even MQCs detected after inserting various delays, and Fig. 4b displays those detected after applying RUDDp sequences of same durations. The first spectrum corresponding to no-delay is same in both cases, in which one can easily observe MQCs of order up to 14. Other spectra in (b) were obtained by RUDDp sequences constructed with increasing number of pulses, i.e., $N = 1, 2, \dots, 7$. Under no DD (Fig. 4a), the intensities decay monotonically with delays, while under RUDDp (Fig. 4b) the dependence of intensities is oscillatory w.r.t. N . Similar behavior was earlier observed in a two-qubit liquid state NMR system [31]. The spectra in (b) at odd N clearly show better intensities compared to the corresponding spectra in (a). Comparisons of performance of different DD schemes for preserving MQCs of various orders are described in the following.

The intensities of MQCs of even orders between 2 and 8 w.r.t. size of various DD schemes are plotted in Fig. 5. Although we can observe MQCs of higher orders than 8 for short durations, for longer durations their intensity measurements are not reliable due to noise. The first data point in each data set corresponds to no DD, and the rest correspond to different size of the DD sequence with $N = 1, 2, \dots, 7$. As observed in Fig. 4b, we see the oscillatory behavior of each MQC under various DD schemes.

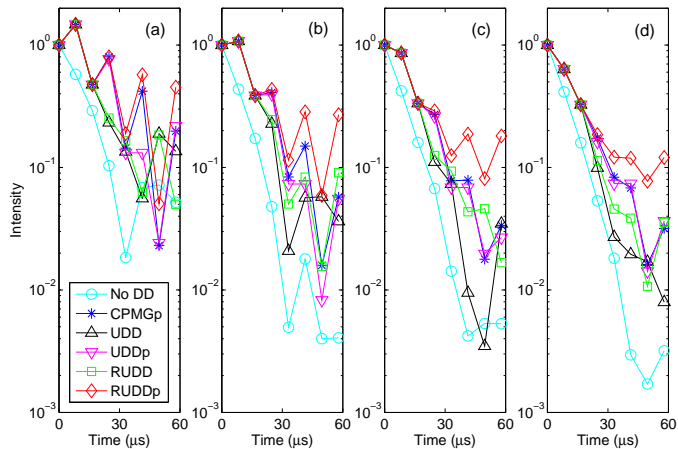


FIG. 5: Performance of various DD schemes in preserving MQCs of order 2 (a), 4 (b), 6 (c), and 8 (d). Each data set has 8 points, in which the first point corresponds to no DD, and the rest correspond to different size of the DD sequences with $N = 1, 2, \dots, 7$.

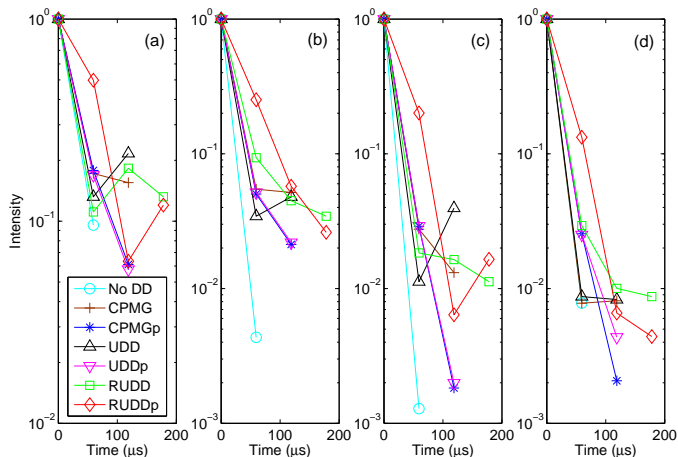


FIG. 6: Performance of various DD schemes in preserving MQCs of order 2 (a), 4 (b), 6 (c), and 8 (d). The intensities were obtained from spectra detected after applying up to a maximum of 3 cycles of 7-pulse DD schemes.

But all the DD schemes display an overall improvement w.r.t. no DD. However it can be noticed that RUDDp has significantly better performance than all other schemes, even for higher order coherences. Surprisingly, unlike the single-quantum case, wherein RUDD displayed the best performance, in multiple-quantum case RUDDp is the best scheme.

The intensities of MQCs of even orders between 2 and 8 for different cycles of 7-pulse DD schemes are plotted in Fig. 6. The first data point in each case corresponds to no DD. The fast decay of magnetization under no DD allowed to detect intensities corresponding to a duration of only one cycle, while for RUDD and RUDDp, intensities up to 3 cycles could be detected.

V. CONCLUSIONS

We studied the performance of various DD schemes on nuclear spins with long-range interactions using a solid state NMR system. First we applied these DD schemes on a single quantum coherence. The experiments were carried out for various 7-pulse DD schemes and for different delays (τ) between the π pulses. The results clearly show that all the DD schemes are able to preserve the single quantum coherence for longer durations of time compared to no DD. However, for small delays between the π pulses, RUDD showed the best performance. For longer delays between the π pulses, CPMG was better. Then we prepared MQCs of even orders using multiple cycles of the well known 8-pulse sequence implementing a two-quantum average Hamiltonian. The MQCs so prepared could be detected using standard spin-counting type experiments. We found the Various DD schemes were inserted after the preparation of MQCs. We studied the performance of these DD sequences with different sizes. The intensity behavior under all the DD sequences were oscillatory. DD sequences with odd number of π pulses showed much better performance than those with even number of π pulses. RUDDp sequence showed the best performance over all other sequences. Since much of the theoretical and experimental work on dynamical decoupling is limited to one or two qubits, we hope that the present work will shed light on the behavior of dynamical decoupling in systems with a large number of correlated qubits. It may also be interesting to study the behavior of odd quantum coherences under DD. It is possible to excite MQCs of all orders (both even and odd) simultaneously using pulse sequences implementing single quantum average Hamiltonians [36].

Acknowledgments

Authors acknowledge useful discussions with Prof. Anil Kumar, Prof. G. S. Agarwal, Dr. Vikram Athalye, Dr. Karthik Gopalakrishnan, and S. S. Roy. The use of 500 MHz NMR spectrometer at NMR Research Center, IISER-Pune is acknowledged.

[1] S. Ding, C. A. McDowell, C. Ye, M. Zhan, X. Zhu, K. Gao, X. Sun, X. Mao, and M. Liu, *Eur. Phys. J. B* **24**, 23 (2001).

[2] G. M. Leskowitz, N. Ghaderi, R. A. Olsen, and L. J. Mueller, *J. Chem. Phys.* **119**, 1643 (2003).

[3] J. Baugh, O. Moussa, A. Ryan, R. Laflamme, C. Ram-

- nathan, T. F. Havel, and D. G. Cory Phys. Rev. A **104**, 22305 (2006).
- [4] O. Moussa et al, C. Ryan, D. Cory, and R. Laflamme, Phys. Rev. Lett. **104**, 160501 (2010).
- [5] S. Simmons, R. M. Brown, H. Riemann, N. V. Abrosimov, P. Becker, H. Pohl, M. L. W. Thewalt, K. M. Itoh, and J. J. L. Morton, Nature **470**, 69 (2011).
- [6] Y. Yen and A. Pines, J. Chem. Phys. **78**, 3579 (1983).
- [7] J. Baum, M. Munowitz, A. N. Garroway, and A. Pines, J. Chem. Phys. **83**, 2015 (1985).
- [8] H. Krojanski and D. Suter, Phys. Rev. A **74**, 062319 (2006).
- [9] M. Lovric, H. Krojanski, and D. Suter, Phys. Rev. A **75**, 042305 (2007).
- [10] G. A. Alvarez and D. Suter, Phys. Rev. Lett. **104**, 230403 (2010).
- [11] H. Y. Carr and E. M. Purcell, Phys. Rev. **94**, 630 (1954).
- [12] S. Meiboom and D. Gill, Rev. Sci. Instr. **29**, 688 (1958)
- [13] L. Viola, E. Knill, and Seth Lloyd, Phys. Rev. Lett. **82**, 2417 (1999).
- [14] G. S. Uhrig, Phys. Rev. Lett. **98**, 100504 (2007).
- [15] M. J. Biercuk, H. Uys, A. P. VanDevender, N. Shiga, W. M. Itano, and J. J. Bollinger, Nature **458**, 996 (2009).
- [16] M. J. Biercuk, H. Uys, A. P. VanDevender, N. Shiga, W. M. Itano, and J. J. Bollinger, Phys. Rev. A **79**, 062324 (2009).
- [17] M.J. Biercuk, A.C. Doherty, and H. Uys, arXiv:1012.4262 (2010). Accepted to Journal of Physics B.
- [18] J. Du, X. Rong, N. Zhao, Y. Wang, J. Yang, and R. B. Liu, Nature **461**, 1265 (2009).
- [19] G. A. Alvarez, A. Ajoy, X. Peng, and D. Suter, Phys. Rev. A **82**, 042306 (2010).
- [20] L. Cywinski, R. M. Lutchyn, C. P. Nave, and S. Das Sarma, Phys. Rev. B **77**, 174509 (2008).
- [21] G. de Lange, Z. H. Wang, D. Riste, V. V. Dobrovitski, and R. Hanson, Science **330**, 60 (2010).
- [22] C. Barthel, J. Medford, C. M. Marcus, M. P. Hanson, and A. C. Gossard, arXiv:1007.4255 (2010).
- [23] C. A. Ryan, J. S. Hodges, and D. G. Cory, Phys. Rev. Lett. **105**, 200402 (2010).
- [24] Yoav Sagi, Ido Almog, and Nir Davidson, Phys. Rev. Lett. **105**, 053201 (2010).
- [25] A. Ajoy, G. A. Alvarez, and D. Suter, Phys. Rev. A **83**, 032303 (2011).
- [26] J. R. West, B. H. Fong, and D. A. Lidar, Phys. Rev. Lett. **104**, 130501 (2010).
- [27] S. Pasini, P. Karbach, and G. S. Uhrig, arxiv: 1009.2638v2, (2010).
- [28] G. S. Agarwal, Phys. Scr. **82**, (2010) 038103.
- [29] M. Mukhtar, W. T. Soh, T. B. Saw, and J. Gong, Phys. Rev. A **82**, 052338 (2010).
- [30] Y. Wang, X. Rong, P. Feng, W. Xu, B. Chong, Ji-Hu Su, J. Gong, and J. Du, Phys. Rev. Lett. **106**, 040501 (2011).
- [31] S. S. Roy and T. S. Mahesh, Phys. Rev. A **82**, 052302 (2010).
- [32] C. P. Slichter, *Principles of Magnetic Resonance*, Third Edition, Springer (1996).
- [33] M. H. Levitt, *Spin Dynamics*, J. Wiley and Sons Ltd., Chichester (2002).
- [34] Y. Dong, R. G. Ramos, D. Li, and S. E. Barrett, Phys. Rev. Lett. **100**, 247601 (2008).
- [35] D. Li, Y. Dong, R. G. Ramos, J. D. Murray, K. MacLean, A. E. Dementyev, and S. E. Barrett, Phys. Rev. B **77**, 214306 (2008).
- [36] D. Suter, S. B. Liu, J. Baum, and A. Pines, Chem. Phys. **114**, 103 (1987).